PLANT SCIENCES

A plant virus manipulates both its host plant and the insect that facilitates its transmission

Peng Liang[1,2]†, Yang Zeng[1,3]†, Jie Ning[1]†, Xiaojie Wu[1], Wenlu Wang[1], Jun Ren[1], Qingjun Wu[1], Xin Yang[1], Shaoli Wang[1], Zhaojiang Guo[1], Qi Su[4], Xuguo Zhou[5], Ted C. J. Turlings[6,7]*, Wen Xie[1,8]*, Youjun Zhang[1]*

Tomato yellow leaf curl virus (TYLCV), a devastating pathogen of tomato crops, is vectored by the whitefly *Bemisia tabaci*, yet the mechanisms underlying TYLVC epidemics are poorly understood. We found that TYLCV triggers the up-regulation of two β-myrcene biosynthesis genes in tomato, leading to the attraction of nonviruliferous *B. tabaci*. We also identified BtMEDOR6 as a key whitefly olfactory receptor of β-myrcene involved in the distinct preference of *B. tabaci* MED for TYLCV-infected plants. TYLCV inhibits the expression of BtMEDOR6, canceling this preference and thereby facilitating TYLCV transmission to uninfected plants. Greenhouse experiments corroborated the role of β-myrcene in whitefly attraction. These findings reveal a sophisticated viral strategy whereby TYLCV modulates both host plant attractiveness and vector olfactory perception to enhance its spread.

INTRODUCTION

Plant viruses that are vectored by insects are estimated to cost more than $30 billion in crop losses each year (*1*). Of the 697 plant viruses recognized by the International Committee on Virus Classification, 76% are transmitted by insects, of which 55% are transmitted by Hemiptera insects (*2*). During the process of seeking and feeding on host plants, insect vectors are often affected by viruses indirectly through the regulation of host plant characteristics that can facilitate more efficient acquisition of the virus by the vectoring insects (*3*). For example, tomato spotted wilt virus can modify plant terpene synthesis by inhibiting the plant jasmonic acid (JA) pathway, resulting in reduced emissions of deterrent volatiles in infected plants, thus increasing their attractiveness to healthy thrips (*4*). Tomato severe rugose virus infects tomato leaves, causing leaf yellowing, which encourages nonviruliferous *Bemisia tabaci* to visit diseased plants (*5*). Cucumber mosaic virus induces cucumbers to produce specific volatiles that attract nonviruliferous aphids to feed on cucumbers (*6*). The βC1 protein of tomato yellow leaf curl China virus directly interacts with the basic helix-loop-helix transcription factor MYC2 to compromise the activation of MYC2-regulated terpene synthase genes, thereby reducing whitefly resistance (*7*). In addition, viruses can modulate the plant phenotype in ways that it renders the host plant unpalatable or less suitable, causing viruliferous insects to leave the infected plant to complete the transmission (*6*, *8*, *9*). A few plant viruses are known to facilitate transmission by manipulating the vector insects themselves, such as tomato yellow leaf curl virus (TYLCV) which causes brain apoptosis in *B. tabaci*, resulting in the loss of their attraction to diseased plants (*10*). A possible combined manipulation of both the host plant and insect vector has not previously been considered.

Plant viruses may affect olfactory signals to influence the behavior of insect vectors and their relationship with host plants. For example, *B. tabaci* orients more actively toward the host plant cucumber when carrying cucurbit chlorotic yellows virus (*11*). Rice black-streaked dwarf virus and Rice stripe virus are able to directly regulate the gene of an odorant-binding protein and olfactory receptor (OR) coreceptor of their insect vectors, changing the vectors' odor preferences from virus infected to uninfected host plants (*12*, *13*). ORs are the core of insect olfactory systems, determining how active volatile molecules stimulate olfactory sensory neurons (*14*, *15*). Thus, insect ORs play an important role in locating host plants, identifying mates, and aggregating populations (*16*–*22*). ORs have also been shown to be of importance for insect vectors. For instance, in the pea aphid *Acyrthosiphon pisum*, which vectors numerous plant viruses, the specific binding of the *ApOR5-ORco* heterocomplex to its activating ligand, geranyl acetate, has recently been unraveled (*23*). *Aedes aegypti*, a vector of viruses that affect human healthy, uses *AaOR8* and the unique OR-ORco to localize human hosts (*24*, *25*). *AaOR4* has also been shown to be specifically associated with the preference for human odors, and a reduction of *AalORco* transcript levels was found to decrease host seeking in *Aedes albopictus* (*26*, *27*).

B. tabaci is one of the most important virus vectoring insects in the world (*28*). It can infest hundreds of crops, particularly vegetables and horticultural crops, and can cause substantial harm through direct feeding and virus spread (*29*). *B. tabaci* Mediterranean (MED) is the most damaging and widespread biotype of the whitefly worldwide (*30*). According to statistics, *B. tabaci* MED can transmit more than 100 species of viruses (*30*), of which TYLCV is one of the most destructive pathogens. Yield losses of up to 100% have been observed in some susceptible tomato varieties, posing a major threat to

[1]State Key Laboratory of Vegetable Biobreeding, Department of Plant Protection, Institute of Vegetables and Flowers, Chinese Academy of Agricultural Sciences, Beijing 100081, China. [2]Institute of Plant Protection, Tianjin Academy of Agricultural Sciences, Tianjin 300381, China. [3]Hubei Key Laboratory of Edible Wild Plants Conservation and Utilization, College of Life Sciences, Hubei Normal University, Huangshi, China. [4]Ministry of Agriculture and Rural Affairs Key Laboratory of Sustainable Crop Production in the Middle Reaches of the Yangtze River (Co-construction by Ministry and Province), Hubei Engineering Technology Center for Pest Forewarning and Management, College of Agriculture, Yangtze University, Jingzhou, Hubei 434025, China. [5]Department of Entomology, School of Integrative Biology, College of Liberal Arts and Sciences, University of Illinois Urbana-Champaign, 505 S. Goodwin Ave., Urbana, IL 61801-3795, USA. [6]State Key Laboratory of Cotton Bio-breeding and Integrated Utilization, School of Life Sciences, College of Agriculture, Henan University, Zhengzhou 475004, China. [7]Laboratory of Fundamental and Applied Research in Chemical Ecology, Institute of Biology, University of Neuchâtel, 2000 Neuchâtel, Switzerland. [8]National Research Institute of Breeding in Hainan, Chinese Academy of Agricultural Sciences, Sanya, Hainan, China.
*Corresponding author. Email: ted.turlings@unine.ch (T.C.J.T.); xiewen@caas.cn (W.X.); zhangyoujun@caas.cn (Y.Zh.)
†These authors contributed equally to this work.

global tomato production (*31*). Various studies have shown that *B. tabaci* MED is key to the global outbreaks of TYLCV (*32*–*34*).

TYLCV has a particularly intriguing mutualistic symbiosis with *B. tabaci* MED. Nonviruliferous *B. tabaci* MED show substantial positive chemotaxis toward TYLCV-infected tomato, whereas virus-carrying *B. tabaci* MED do not show this attraction (*10*, *35*). As suggested by the "conditional vector preference" hypothesis (*36*, *37*), this change in odor preference may greatly accelerate the spread of TYLCV. The underlying mechanism has not yet been elucidated. In this study, we aimed to understand the molecular mechanisms behind the apparent manipulation of the virus of the host plant odor and the whitefly's odor preference. We present conclusive evidence that TYLCV modulates tomato-derived volatile cues that attract vectoring whiteflies and also manipulates the vectors' olfactory system to accelerate the rate at which they acquire and transmit TYLCV.

RESULTS

B. tabaci MED prefer TYLCV-infected tomato mainly through β-myrcene

When given a choice in an observation cage (fig S1A), nonviruliferous *B. tabaci* MED preferred TYLCV-infected to healthy tomato plants (Fig. 1A and fig. S1B), which is in accordance with previous studies (*10*, *36*). Since host plant localization by herbivorous insects is closely related to olfactory perception, we conducted additional choice experiments to test the whitefly's odor preferences (fig. S2). Nonviruliferous whiteflies, when given a choice between the odors of healthy versus infected tomato plants, preferred the odor of TYLCV-infected tomato plants (Fig. 1B).

Next, the volatiles contained in healthy/uninfected and TYLCV-infected tomatoes were analyzed using gas chromatography–mass spectrometry (GC-MS), which yielded 12 volatiles that were significantly different between them (Fig. 1C and table S1). Choice tests were used to test the attractiveness of each volatile to nonviruliferous *B. tabaci* MED, which revealed that, at a concentration of 2000 ng/μl, they were only significantly attracted to β-myrcene and β-cymene, whereas α-humulene was found to be repellent (Fig. 1D). When we reduced the concentrations of β-myrcene and β-cymene, we found that nonviruliferous *B. tabaci* MED were also attracted to β-myrcene at concentrations of 200 and 20 ng/μl (Fig. 1E), but β-cymene was no longer attractive (Fig. 1G).

Choice tests were then used to determine to what extent β-myrcene and β-cymene affect the attractiveness of nonviruliferous *B. tabaci* MED to TYLCV-infected tomatoes. The addition of β-myrcene (2000 or 200 ng/μl) to healthy tomato plants made them as attractive to *B. tabaci* MED as TYLCV-infected tomato plants (Fig. 1F). In contrast, spiking healthy plants with β-cymene had no effect on the choices made by nonviruliferous *B. tabaci* MED, which still favored TYLCV-infected plants (Fig. 1H).

We also found that there was a significant difference in the contents of β-myrcene between healthy and TYLCV-infected tomato leaves (Fig. 1, I and J), with β-myrcene (about 213 and 446 ng/g) in healthy tomato and TYLCV-infected tomato, respectively (Fig. 1K).

TYLCV manipulates tomato *TPS3* and *TPS7* gene expression to attract nonviruliferous *B. tabaci* MED

TPS3 and *TPS7* genes play key function in controlling β-myrcene synthesis in tomato (*38*). A significant increase in gene expression of *TPS3* and *TPS7* was observed in TYLCV-infected tomatoes compared to healthy plants (Fig. 2A). Knockout tomatoes for *TPS3* and *TPS7* ($TPS3^{-/-}$ and $TPS7^{-/-}$) were successfully constructed using CRISPR-Cas9 technology, which did not differ from wild tomato in phenotype and growth rate (Fig. 2, B and C, and fig. S3). As expected, healthy (Fig. 2D) and TYLCV-infected knockout tomatoes (Fig. 2E) did not produce any detectable amounts of β-myrcene, unlike wild-type (WT) plants.

In addition, a free choice test showed that nonviruliferous *B. tabaci* MED tended to prefer WT over knockout tomatoes (Fig. 2F), even if TYLCV infected (Fig. 2G). Spiking the knockout plants with β-myrcene made them as attractive to nonviruliferous *B. tabaci* MED as WT tomato (Fig. 2H), and *B. tabaci* MED did not distinguish between uninfected and TYLCV-infected knockout tomato (Fig. 2I).

BtMEDOR6 is involved in the detection of β-myrcene and the attraction to TYLCV-infected tomato plants

Nonviruliferous *B. tabaci* MED preferred TYLCV-infected tomato plants, while viruliferous *B. tabaci* MED do not make this distinction in free choice tests (Fig. 3A). This implies that TYLCV interferes with *B. tabaci* MED's preference for TYLCV-infected tomato plants and suggests a manipulation of the whitefly's odor perception.

On the basis of the genome and transcriptome data of *B. tabaci*, we identified a total of 10 olfactory receptor genes including a conserved *ORco* gene (table S2 and fig. S4), all highly expressed in the head and particularly in adult females (figs. S4 and S5). Six OR genes showed significant down-regulation in viruliferous *B. tabaci* MED relative to nonviruliferous *B. tabaci* MED (Fig. 3B). The subsequent free-choice experiments after RNA interference (RNAi) showed that nonviruliferous *B. tabaci* MED adults no longer preferred TYLCV-infected tomatoes after knocking down the expression of *BtMEDOR6* (Fig. 3C and fig. S6), implying that they had lost their ability to detect β-myrcene (Fig. 3D).

Western blot analyses revealed that the protein levels of the *BtMEDOR6* gene decreased substantial after *BtMEDOR6* interference, which were consistent with the measured mRNA levels (Fig. 3, E and F). We also measured the *BtMEDOR6* protein levels in *B. tabaci* after acquisition of TYLCV during a 7-day period and found a substantial decrease in *BtMEDOR6* expression which was most evident on the fifth day after acquisition of TYLCV (Fig. 3, G and H). We also exposed nonviruliferous *B. tabaci* MED to different odor blends with or without β-myrcene and found that the expression of *BtMEDOR6* gene was significantly up-regulated in response to β-myrcene (fig. S7). Last, the experiment with *Xenopus oocytes* revealed that the specific function of the *BtMEDOR6*/*ORco* system is to perceive β-myrcene and that the magnitude of the response value to β-myrcene correlated with its concentration (Fig. 3, I and J).

The Y204F in BtOR6 affecting OR receptor binding to β-myrcene

Among the four tested different *B. tabaci* subspecies, only nonviruliferous *B. tabaci* MED was attracted to TYLCV-infected tomato plants (Fig. 4A and fig. S1). In the previous section, we confirmed that *OR6* was the key gene in *B. tabaci* MED involved in this preference (Fig. 3). The genome analyses and transcriptome data found no homologous gene of *BtMEDOR6* in *B. tabaci* AsiaII6, and the cloned *OR6* gene of *B. tabaci* Asia1 showed a large deletion compared to the *B. tabaci* MED gene (Fig. 4B and fig. S8). Sequence similarity of *OR6* between *B. tabaci* Middle East-Asia Minor 1 (MEAM1) and MED is

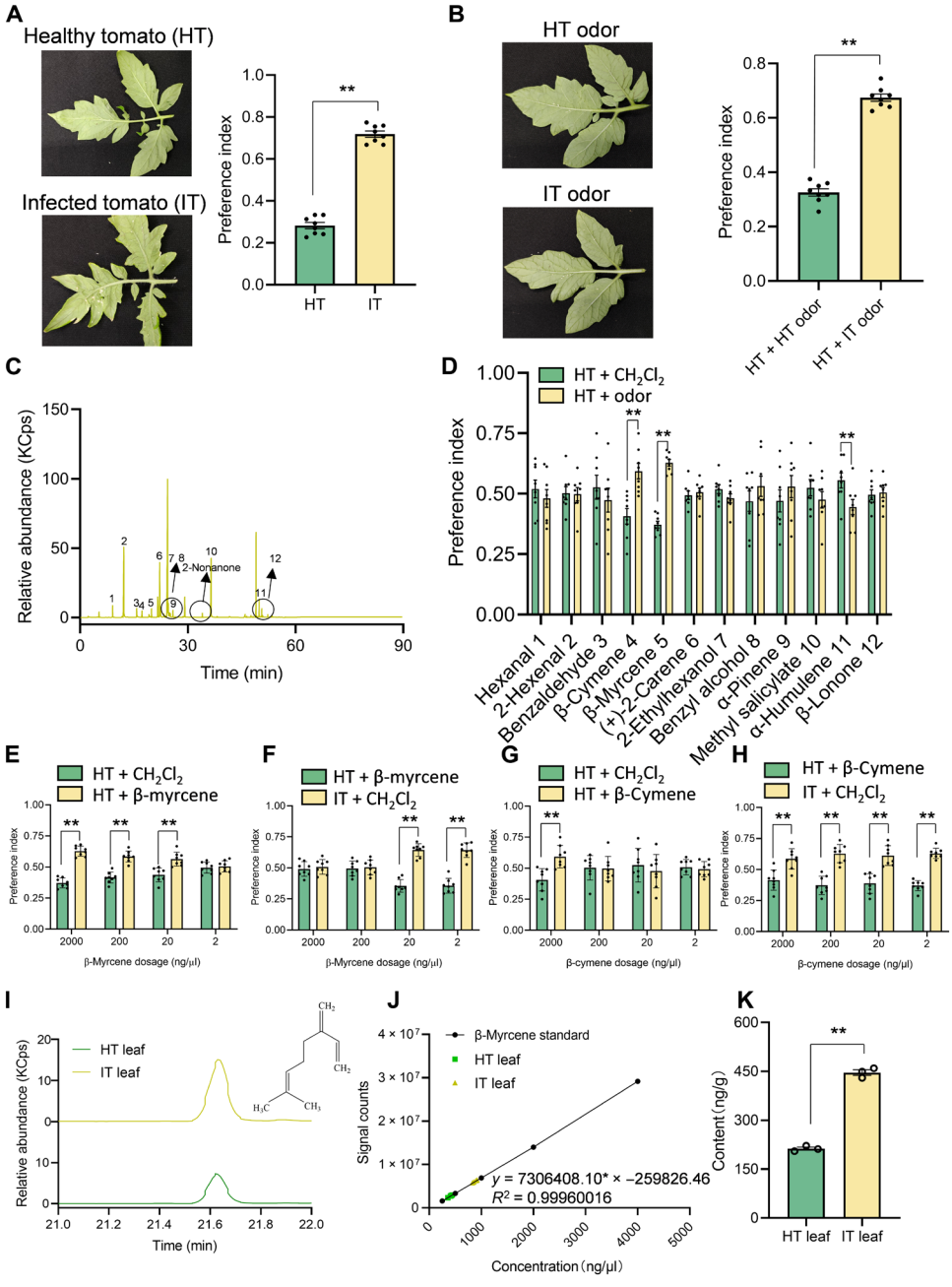

Fig. 1. Nonviruliferous *B. tabaci* MED prefer to settle on TYLCV-infected tomato plants which can be attributed to enhance release of β-myrcene. (**A** and **B**) The choices of *B. tabaci* MED when offered a choice between healthy and TYLCV-infected tomato plants (A) or the volatiles collected from such plants (B) ($n = 8$, t test, $^{**}P < 0.01$). (**C**) Chromatogram of volatiles collected from TYLCV-infected tomato plants (numbers represent 12 compounds that differ in emitted quantities between TYLCV-infected and uninfected tomato plants; see table S1. 2-Nonanone is an internal standard). (**D**) The responses of *B. tabaci* MED to each of these volatiles ($n = 8$, t test, $^{*}P < 0.05$, $^{**}P < 0.01$, and $^{***}P < 0.001$). (**E** and **G**) The choices of *B. tabaci* MED for the odor of healthy plants spiked or not with β-myrcene (E) or β-cymene (G) at different concentrations ($n = 8$, t test, $^{*}P < 0.05$, $^{**}P < 0.01$, and $^{***}P < 0.001$). (**F** and **H**) The choices of *B. tabaci* MED for the odor of healthy plants spiked with β-myrcene (F) or β-cymene (H) at different odor concentrations versus the odor of infected plants ($n = 8$, t test, $^{*}P < 0.05$, $^{**}P < 0.01$, and $^{***}P < 0.001$). (**I**) Chromatograms showing the peak of β-myrcene for TYLCV-infected and uninfected tomato leaves. (**J** and **K**) Standard curve for β-myrcene (J) and its actual content quantity in TYLCV-infected and uninfected tomato leaves (K) ($n = 3$, t test, $^{*}P < 0.05$, $^{**}P < 0.01$, and $^{***}P < 0.001$). HT, healthy tomato; IT, TYLCV-infected tomato. "*n*" indicates the number of biological replicates, and the number of whiteflies used per biological replicate was about 60.

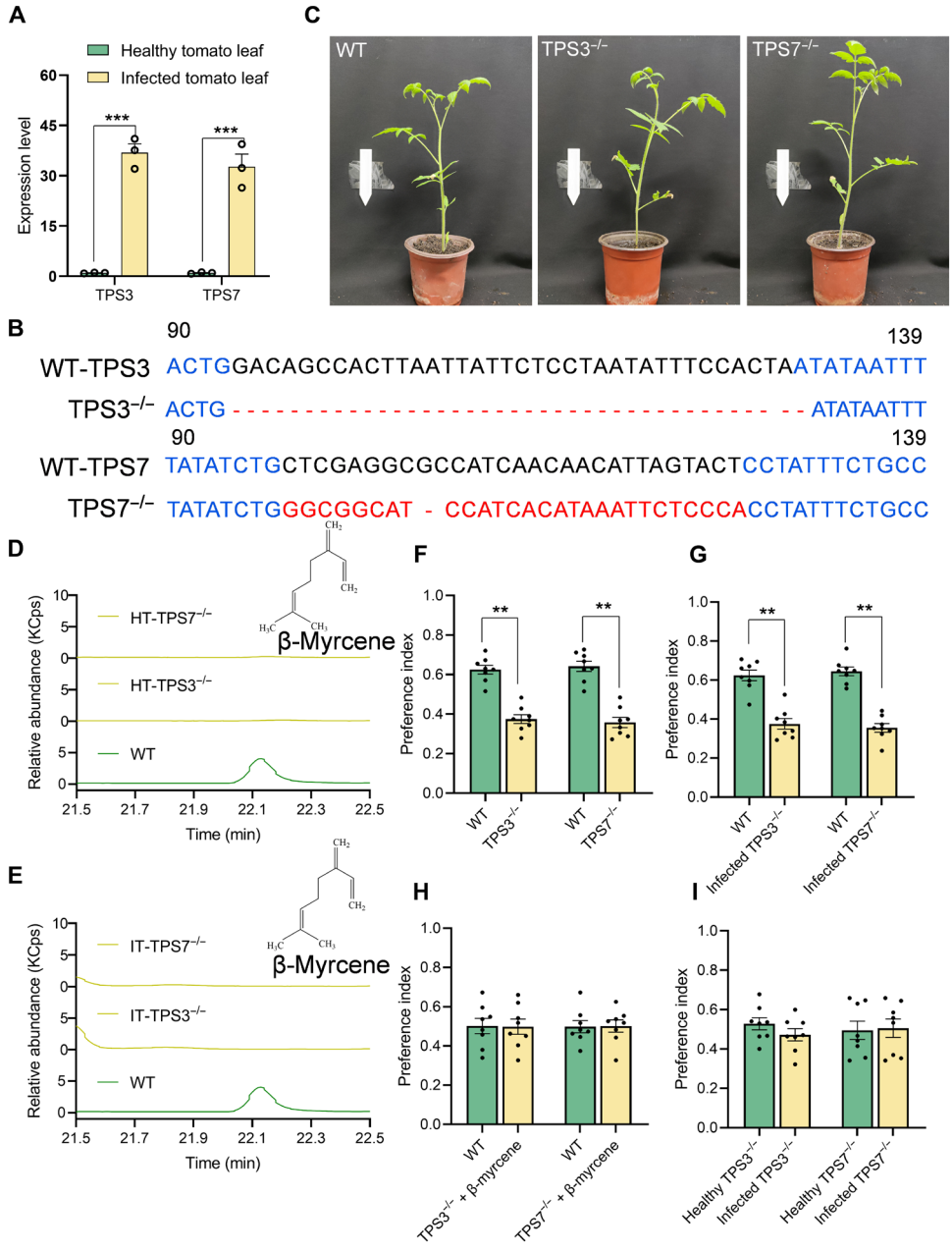

Fig. 2. *TPS3* and *TPS7* determine the production of β-myrcene and thereby the attractiveness of tomato plants to *B. tabaci* MED. (**A**) Expression levels of *TPS3* and *TPS7* genes in TYLCV-infected and uninfected tomatoes (n = 3, t test, and ***P < 0.001). (**B**) Knockout targets for *TPS3* and *TPS7*. (**C** and **D**) Phenotypic (C) and β-myrcene content (D) differences after successfully knocking out *TPS3* and *TPS7* (WT: healthy AC tomato). (**E**) Comparative β-myrcene content of TYLCV-infected knockout tomatoes ($TPS3^{-/-}$ and $TPS7^{-/-}$). (**F**) The choices of *B. tabaci* MED between the WT and knockout tomato plants ($n = 8$, *t* test, $^{**}P < 0.01$). (**G**) The choices of *B. tabaci* MED between TYLCV-infected knockout and healthy WT tomato plants ($n = 8$, *t* test, $^{**}P < 0.01$). (**H**) The choices of *B. tabaci* MED between the WT and knockout tomato plants spiked with β-myrcene ($n = 8$, *t* test). (**I**) The choices of *B. tabaci* MED between healthy and TYLCV-infected knockout tomato plants ($n = 8$, *t* test). "*n*" indicates the number of biological replicates, and the number of whiteflies used per biological replicate was about 60.

99.9%, and only Y204F made the difference (Fig. 4B and fig. S9). Site mutations often result in structural changes, which can lead to changes in protein function.

The three-dimensional modeling of the OR6 protein structure revealed that the Y204F mutation exerts an effect on the local three-dimensional conformation within the *BtMEAM1OR6* (fig. S10). Molecular dynamic (MD) simulations showed that the *BtMEDOR6* protein exhibits high structural stability, characterized by a marked increase in the number of intramolecular hydrogen bonds formed between amino acids, as compared to the *BtMEAM1OR6* protein (fig. S11). Further insights from molecular docking analysis revealed that the Y204F mutation led to a decrease in the amino acid count engaged in hydrophobic interactions proximal to site 204 in *BtMEAM1OR6*, alongside an elongation of the average hydrogen

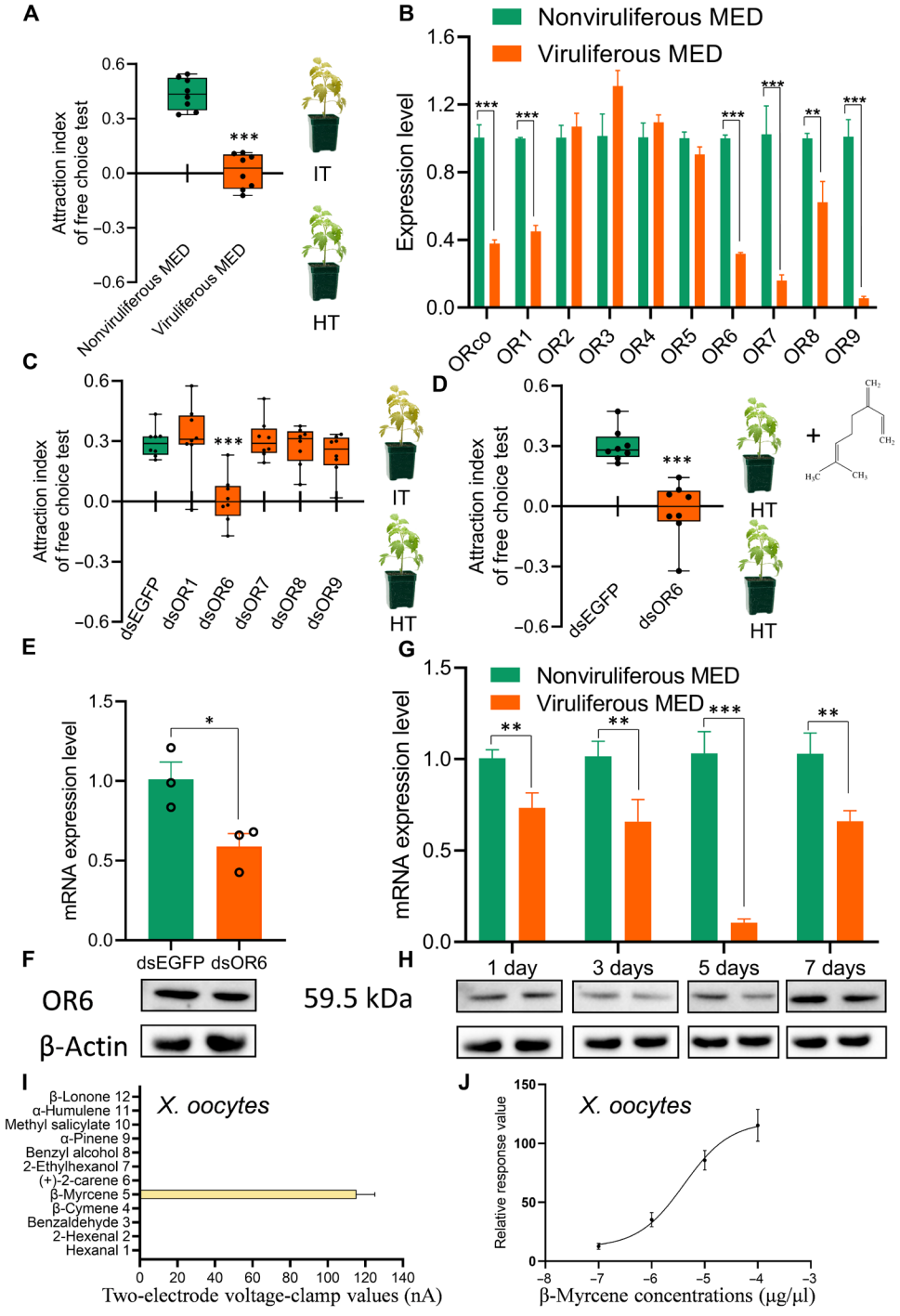

Fig. 3. The key role of *OR6* in allowing nonviruliferous *B.tabaci* MED to perceive β-myrcene emitted by TYLCV-infected tomato plants. (**A**) Nonviruliferous *B. tabaci* MED preferred TYLCV-infected tomatoe plants. (**B**) Differential gene expression of ORs comparing nonviruliferous and viruliferous *B. tabaci* MED. ($n = 3$, *t* test, $^{**}P < 0.01$ and $^{***}P < 0.001$). (**C** and **D**) Only the interference with *OR6* in nonviruliferous *B. tabaci* MED resulted in losing the preference for infected tomato plants (C) and healthy tomato plants spiked with β-myrcene (D) ($n = 8$, *t* test, $^{***}P < 0.001$). (**E** and **F**) Changes in mRNA (E) and protein levels (F) of *BtMEDOR6* after 48 hours of interference ($n = 3$, *t* test, $^{*}P < 0.05$). (**G** and **H**) Changes in mRNA (G) and protein levels (H) of *BtMEDOR6* after virus acquisition for 7 days ($n = 3$, *t* test, $^{**}P < 0.01$ and $^{***}P < 0.001$). (**I** and **J**) Two-electrode voltage-clamp values of *OR6*/*ORco* ectopically expressed in *Xenopus* oocytes by exposure to different volatiles (I) or different concentrations of β-myrcene (J) ($n = 3$). MED, *B.tabaci* MED.

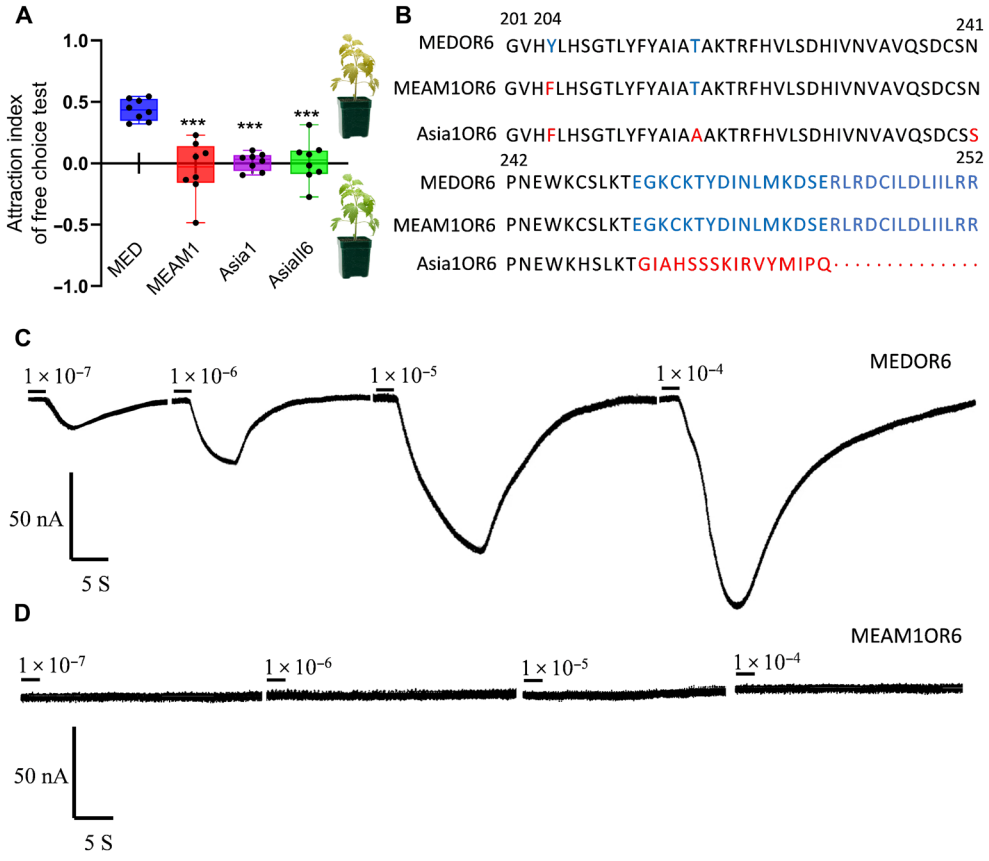

Fig. 4. The Y204F in BtOR6 affecting OR receptor binding to β-myrcene. (**A**) The responses of four *B. tabaci* species to the TYLCV-infected tomato ($n = 8$, *t* test, ***$P <$ 0.001, * indicates differences in preference choices for *B.tabaci* MED and the choices made by the three other whitefly populations). (**B**) Sequence analysis of *OR6s* of *B. tabaci* Asia1, MEAM1, and MED. (**C** and **D**) Two-electrode voltage-clamp values of *BtMEDOR6/ORco* (C) or *BtMEAM1OR6/ORco* (D) ectopically expressed in *Xenopus* oocytes upon different concentrations of β-myrcene exposure. MEAM1, *B. tabaci* MEAM1; Asia1: *B.tabaci* Asia1; AsiaII6: *B.tabaci* AsiaII6.

bond distances. This perturbation disrupted the binding pocket adjacent to site 204, potentially affecting the interaction with β-myrcene molecules (fig. S12). The outcome of the docking analysis suggests that the pocket housing the Tyr^{204} residue within the *BtMEDOR6/ORco* tetramer architecture represents the most probable site for stable β-myrcene binding, whereas this crucial pocket seems to be absent in the *BtMEAM1OR6/ORco* complex (figs. S13 and S14 and tables S3 and S4).

Subsequent experiments with *Xenopus laevis* oocytes confirmed that *BtMEAM1OR6/ORco* did not respond to β-myrcene stimulation (Fig. 4, C and D, and fig. S15). These results confirm that the Y204F between *B. tabaci* MED and MEAM1 likely resulted in the binding difference of *BtMEDOR6/ORco* and *BtMEAM1OR6/ORco* to β-myrcene.

β-Myrcene attracts *B. tabaci* MED in greenhouses

To verify the attractive effect of β-myrcene on *B. tabaci* MED in the field, we conducted trapping experiments in tomato greenhouses in three different regions around Beijing (Fig. 5, A and B). Across eight blocks selected on the basis of tomato varieties and time periods, we quantified the number of *B. tabaci* MED captured on CH_2Cl_2 + β-myrcene and control (CH_2Cl_2) sticky boards, CH_2Cl_2 + β-myrcene always significantly attracted more *B. tabaci* adults relative to control (CH_2Cl_2) (Fig. 5C). In addition, the average number of captured *B. tabaci* per board in the CH_2Cl_2 + β-myrcene groups from eight blocks was significantly higher than that in the control groups (Fig. 5D).

DISCUSSION

Understanding the mechanisms by which plant viruses modulate the physiology and behavior of their insect vectors is critical to deciphering the spread and epidemiology of the viruses in the field (*1*, *2*, *36*, *37*, *39*). In this study, we show that TYLCV infection significantly increases the attractiveness of tomato plants to nonviruliferous *B. tabaci* MED by eliciting the emission of the monoterpene β-myrcene (Figs. 1 and 2). We further identified *BtMEDOR6* as the olfactory receptor for β-myrcene in *B. tabaci* MED and demonstrated the critical role of this receptor in determining the host plant choices by the whitefly (Figs. 3 to 5). After acquiring TYLCV, the transcript and protein levels of *BtMEDOR6* were substantially down-regulated, after which viruliferous *B. tabaci* MED no longer preferred to settle on infected plants, thus facilitating the spread of the virus (Fig. 6). These results reveal a unique two-tiered pull-push strategy in which TYLCV maximizes transmission by modulating terpene release from host plants as well as the olfactory system of its vector.

Plant viruses have previously been shown to influence vector behavior by manipulating the production of plant volatiles in their shared

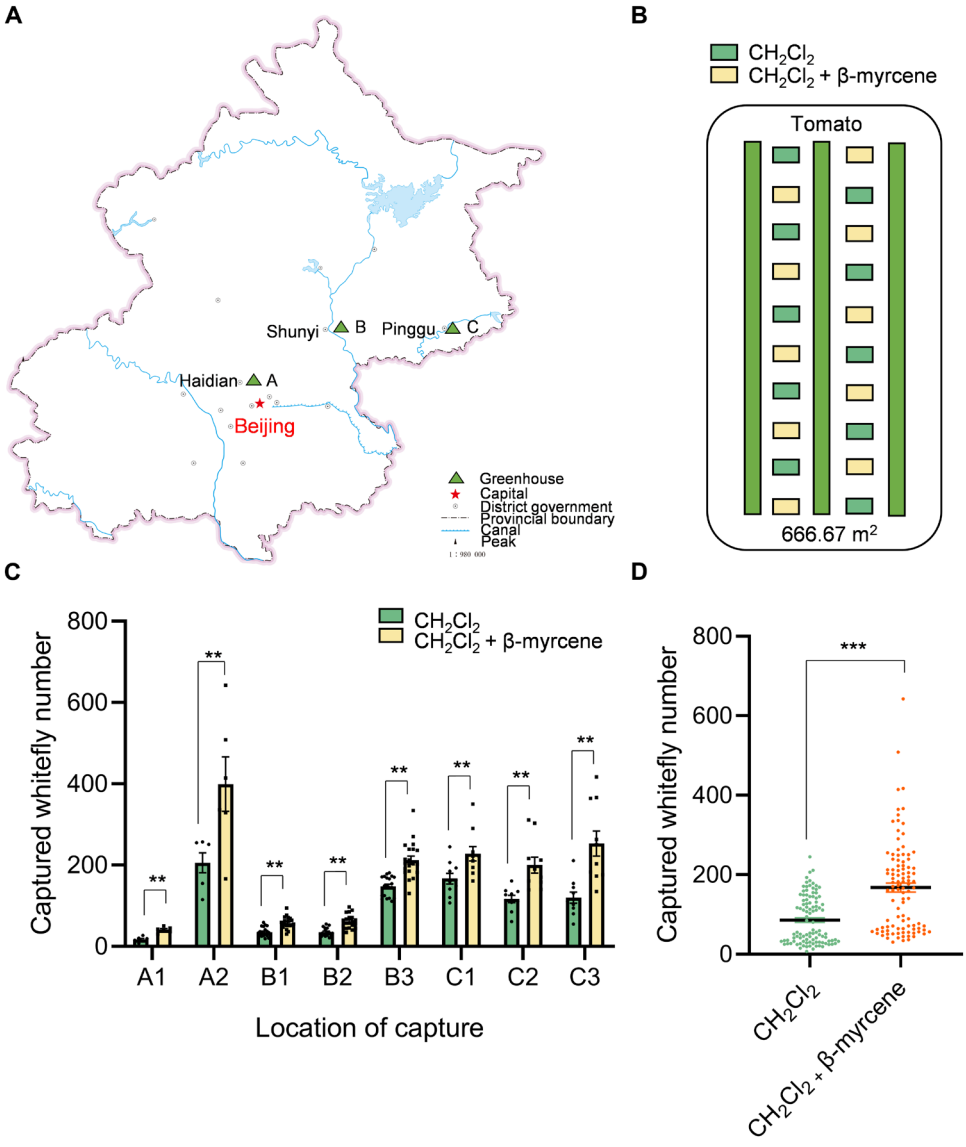

Fig. 5. Attraction of *B. tabaci* to β-myrcene in tomato greenhouses. (**A**) Locations of the selected greenhouses ("A," "B," and "C": Haidian, Shunyi, and Pinggu). (**B**) Schematic design of the field trapping experiment used for each greenhouse, showing the placement of the 20 sticky boards. (**C**) The number of *B. tabaci* captured in the control plots (CH_2Cl_2) and β-myrcene plots after 1 day in eight blocks [the eight different greenhouses were located at three locations, A, B, and C, shown in (A)] ($n \geq 5$, *t* test, $^{**}P < 0.01$). (**D**) The average number of captured *B. tabaci* per board in the β-myrcene group was higher than in the control group ($n = 70$ boards, *t* test, $^{***}P < 0.001$).

host plants (*40*–*42*). A different odor collection method has a large impact on both the type and content of collected odors in related research (*35*, *43*). In this study, we used the more stable solid-phase microextraction (SPME) method and found a significant increase in β-myrcene content in TYLCV-infected tomato plants. We found that TYLCV does this by modulating the expression of two terpene synthesis genes, *TPS3* and *TPS7*, thereby enhancing the emission of whitefly-attracting β-myrcene in tomato plants. When we knocked out the *TPS3* and *TPS7* genes, there were no significant changes in the physiological development of the tomato plants, but β-myrcene was undetectable. This absence of β-myrcene resulted in the inability of the *B. tabaci* MED to distinguish between tomato plants before and after virus infection. Typically, the master regulator MYC2 of the JA signaling pathway controls the formation of homodimers or heterodimers that bind to cis-regulatory elements of target gene promoters, such as terpene synthase (TPS) (*44*–*46*). It has been shown that the pathogenesis factor βC1 of tomato yellow leaf curl China virus regulates *AtTPS3* and represses the JA pathway in *Arabidopsis* by disrupting the dimerization of MYC2 (*7*). The effect on the JA signaling pathway and expression of TPSs observed in TYLCV-infected tomato suggest that TYLCV might also have evolved the capacity to modulate the emission of β-myrcene through the same target but by a different viral protein, as the TYLCV genome lacks the beta satellite βC1 (Fig. 2) (*47*, *48*). Further investigations are needed to determine which protein TYLCV convergently evolved to modulate JA signaling and terpene emission in a manner that is similar to βC1.

The olfactory system enables insects to perceive a wide spectrum of external chemical cues and signals, including plant volatiles

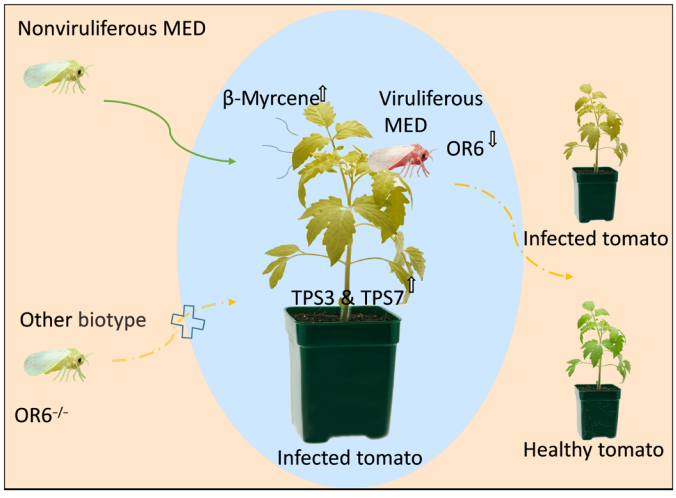

Fig. 6. TYLCV facilitates it spread by manipulating the emission of β-myrcene in tomato plants as well as the β-myrcene receptor *BtMEDOR6* in a vectoring whitefly species.

(*16*–*21*). Each insect species has evolved a specific OR repertoire that is adapted to its specific environment and needs (*49*–*51*). As a rapidly evolving complex of species, the wide variety *B. tabaci* species are quite remarkable in their diversity of such adaptations (*52*, *53*). Nonviruliferous *B. tabaci* MED, for instance, are attracted to volatiles emitted by TYLCV-infected plants, whereas other species of the same complex are not (*10*, *36*). This can be explained by the evolved divergence of OR genes in different populations of *B. tabaci*. We here show that *BtMEDOR6* binds specifically to virus-induced β-myrcene emitted by tomato plants, and variations in the *OR6* gene at position 204 prevent this binding of β-myrcene in other species, which, unlike *B. tabaci* MED, do not exhibit a preference for TYLCV-infected tomato plants (Fig. 4). This observation further clarifies the differential ability in virus transmission among the rapidly evolving complex of *B. tabaci* species and is likely to be one of the reasons for the correlation between TYLCV outbreaks and the spread of *B. tabaci* MED (*33*–*35*).

It is commonly found that plant viruses increase the rate of virus transmission by modulating the phenotype of the host plant, which drives the insect vectors that have acquired the virus away from the virulent plant (*6*, *8*, *9*). Recent studies have shown that plant viruses can also have a direct effect on their insect vectors. This makes the relationship between these plant viruses and insect vectors similar to "parasitism" (*40*). For example, satellite RNA of CMV accelerates wing formation in its aphid vector thereby enhancing virus spread (*54*). In our study, TYLCV was found to directly hijack the *BtMEDOR6* gene of whiteflies, causing them to lose the ability to detect the chemical cue β-myrcene, which should enhance visits and transmission to noninfected plants. In a recent study related to ours, it was found that TYLCV-induced apoptotic neurodegeneration in whiteflies, causing insensitivity of *B. tabaci* MED to TYLCV-infected plants (*10*). Both the olfactory receptor and neural system are key in determining the odor-mediated behavior of *B. tabaci* MED adults. How TYLCV manipulates both systems and in what order the manipulation takes place are questions that deserve further investigation. Further research into the mechanistic details of the manipulation steps should also reveal if the insect vector too benefits from these processes.

As the second most important insect pest worldwide and a vector of a large number of plant viruses, *B. tabaci* forms a serious threat to global agricultural production (*28*–*30*). Our current findings provide clues for the development of methods for predicting and controlling outbreaks of *B. tabaci*. For instance, the incorporation of β-myrcene into certain *B. tabaci* trapping devices such as yellow sticky traps might enhance their efficacy in capturing *B. tabaci*. In addition, the identification of the *BtMEDOR6* receptor holds promise for the development attractants to specifically trap *B. tabaci* MED, which might substantially reduce the reliance on chemical insecticides.

Manipulating the behavior of insect vectors is one of the most effective strategies used by plant viruses to enhance their spread (*36*, *40*). We show here that TYLCV not only modulates the emission of plant volatiles to indirectly attract *B. tabaci* MED for virus acquisition but also hijacks the receptor gene *BtMEDOR6* of the vector to change its host plant preference to promote virus spread. Functional analyses will allow us to elucidate how viral elicitors and effectors affect plant volatile emissions and the vector olfactory system. Such approaches have great potential for the development of previously unidentified strategies for the management of vectors and plant pathogens through a genetic engineering approach (*32*, *55*).

MATERIALS AND METHODS

Insects, TYLCV, and plants

The *B. tabaci* MED, *B. tabaci* MEAM1, *B. tabaci* Asia1, and *B. tabaci* AsiaII6 populations used in this study were cultivated on cotton (*Gossypium hirsutum* cv Guo-Shen 7886) enclosed in insect-proof cages in a controlled glasshouse environment at a temperature of 27° ± 1°C, relative humidity between 60 and 80%, and a photoperiod of L16:D8. All four populations of *B. tabaci* are known to acquire and transmit TYLCV. To ensure the genetic integrity of each *B. tabaci* population, a fragment of the *mitochondrial cytochrome oxidase I* gene was sequenced every three to five generations (*56*).

The infectious clone of TYLCV isolate SH2, with GenBank accession number AM282874, was provided by X. Zhou from the State Key Laboratory for Biology of Plant Diseases and Insect Pests at the Institute of Plant Protection, Chinese Academy of Agricultural Sciences. Tomatoes (*Solanum lycopersicum* cv Moneymaker) ("Zhong Za 9") were used as natural hosts for both TYLCV and whitefly in behavioral assays, grown at 27° ± 1°C with 60% relative humidity and a 16:8-hour (light/dark) photoperiod. Tomato seedlings were inoculated with the TYLCV clone by manual injection at the three to four true leaf stages, and after 21 days, only plants with both obvious symptoms and a positive result in polymerase chain reaction (PCR) analyses were used as TYLCV-infected plants for subsequent experiments.

The Ailsa Craig tomato variety was used to generate knockout of the *TPS3* and *TPS7* genes via CRISPR-Cas9. The CRISPR-Cas9 vectors targeting sites in the *TPS3*/*TPS7* exons were designed using the CRISPR-P v2.0 tool (http://cbi.hzau.edu.cn/CRISPR2/). Then, synthetic primers were used to amplify the sgRNAX_U6-26t_SlU6p_ sgRNAX fragment using the pCBC-DT1T2_SlU6p vector as a template. Subsequently, the purified fragments were cloned into pTX041 at the Bsa I sites. Last, the correctly sequenced CRISPR-Cas9 vectors were transformed into Ailsa Craig tomato variety using the agrobacterium-mediated leaf disc transformation method. The transgenic lines were confirmed by PCR and Sanger sequencing. The PCR primers used for transgenic line determination are listed in

table S5. All experiments were performed using homozygous lines from the T2 generation without transferred DNA integration.

Assays with *X. laevis* oocytes

Vectors (pT7TS) carrying full-length olfactory receptor (OR) sequences were used to synthesize complementary RNAs (cRNAs) using the mMESSAGE mMACHINE T7 Kit (Ambion) according to the manufacturer's instructions. Adult female *X. laevis* frogs (>3 years old) were raised in a box with purified water at 18° to 21°C and fed on pig liver. Oocytes were surgically collected before the experiment. After overnight incubation in an incubator at 18°C, oocytes were microinjected with 25 ng of Or cRNA and 25 ng of Orco cRNA, and whole-cell currents in response to volatile exposure were recorded using the two-electrode voltage-clamp technique. Signals were amplified by a two-electrode voltage clamp. The OR responses to 12 different compounds were recorded and analyzed. Data acquisition and analysis were performed using a Digidata 1440A and pCLAMP 10.6 software (Axon Instruments) (*57*). These experiments were conducted under the license of the Animal Experimental Committee of the Institute of Zoology, Chinese Academy of Science (IOZ20170071).

Behavioral assays

Both nonviruliferous and viruliferous whitefly adults that were 3 to 5 days old were respectively used for behavioral experiments. About 60 adults for each treatment were collected in a clean pipet tip as a biological replicate, and eight biological replicates were set up for each experiment. The free-choice tests were conducted in a special behavioral observation box (90 cm by 46 cm by 70 cm; fig. S1A) with healthy/uninfected versus odor-spiked healthy/uninfected, healthy/uninfected versus TYLCV-infected tomato seedlings that were diagonally placed in the box.

For odorant addition, two vials (11.6 mm by 32 mm), one containing an odorant in 100 μl of dichloromethane and the other only with 100 μl of dichloromethane, were placed on the soil with the different plants. Depending on the experiment, we tested an odorant (2000, 200, 20, or 2 ng/μl). To ensure slow release of the volatile compounds, the sample bottles were filled with 100 mg of glass wool, and a glass capillary tube (0.8 mm inner diameter, 2 cm length) was pushed through the septum of the bottle cap (*58*). The attractiveness of tomato and odorants was quantified using a whitefly preference index (PI) calculated as $PI = R$ or $L/(R + L)$, where R is the number of whiteflies choosing the right tomato and L is the number of whiteflies choosing the left tomato. The host selection rate was tested by repeated-measures analysis of variance (ANOVA) (*36*).

For the olfactory related dual-choice assay, two hermetically sealed glass vessels (60 cm in height, 30 cm in diameter) that contained the test plants were connected to two opposite sides of a behavioral observation box (fig. S2). A purified airflow was equally and continually pumped from the glass chamber to the observation box at 500 ml/min (*10*).

In this case, whitefly preference was quantified with an attraction index (AI), calculated as $AI = (V - N)/(V + N)$, where V is the number of whiteflies moving toward virus-infected plants and N is the number of whiteflies moving toward healthy plants in the same experiment (*59*).

Chemical analyses

SPME and GC-MS were used to determine differences in odor emissions among tomatoes that were subjected to different treatments. Two grams of leaves was taken from a mixture of tomato plants, and immediately after removing the leaves, they were placed in a mortar containing liquid nitrogen and ground to a powder. The powdered leaves were then transferred to a 15-ml vial, and 0.6 g of NaCl and 50 μl of 2-nonanone at a concentration of 1025 ng/μ; were added. The vial was heated in water for 10 min at a temperature of 50°C after adding a magnetic stir bar. An SPME fiber was kept at 250°C for 10 min, then was inserted into the vial, and sampled for 40 min. After this, the fiber was immediately inserted into the GC-MS injection port, and the injection program was started.

A 30-m HP-5MS column (Agilent, Santa Clara, CA) was used for the separation of volatiles. The column length was 30 m, diameter of 0.25 mm, film thickness of 0.25 μm, helium as carrier gas, flow rate of 1 ml/min, split ratio of 2:1, and inlet temperature of 250°C. The column temperature was kept at 40°C for 5 min, then warmed up to 120°C at 2°C/min and lastly warmed up to 290°C at 10°C/min, and kept at 290°C for 29 min. The mass range of the mass spectrometer was 35 to 400 mass/charge ratio, and the scanning speed was 781 u/s. The mass spectrometer was scanned at a temperature of 40°C for 5 min. A Bruker chemical analysis MS workstation (MS Data Review, Data Process v.8.0) was used to analyze and process the data (*60*). Mixed samples consisting of standard compounds (purities ≥ 95%; Sigma-Aldrich) at different dosages (250, 500, 1000, 2000, and 4000 ng/μl) were used as external standards to develop the standard curves to quantify the volatiles.

RNA isolation and cDNA synthesis

Total RNA from *B. tabaci* MED was extracted using TRIzol reagent (Ambion); RNA integrity was determined by agarose gel electrophoresis, and RNA quantities were determined using a NanoDrop 2000c spectrophotometer (Thermo Fisher Scientific). cDNA was synthesized using the PrimeScript II First-Strand cDNA Synthesis Kit (Takara) and the PrimeScript RT Kit (including genomic DNA Eraser, Perfect Real Time) (Takara), and samples were stored at −20°C until use.

Gene identification and cloning

The OR genes were identified on the basis of previously sequenced *B. tabaci* MED genome (*61*). The specific primers for gene cloning were designed using Primer Premier 5.0 (table S3). The PCR amplifiers were cloned into the pEASY-T1 vector (TransGen) and transformed into *Escherichia coli* Trans1-T1 competent cells (TransGen) for sequencing (*62*).

qPCR analysis

Gene-specific primers for real-time quantitative PCR (qPCR) analysis were designed with Primer Premier 5.0 (table S4). The 25-μl PCR reaction included 0.5 μl of 50× Rhodamine X (ROX) Reference Dye (TIANGEN), 0.75 μl of each specific primer, 1 μl of cDNA template, 9.5 μl of double distilled water (ddH_2O), and 12.5 μl of 2× SuperReal PreMix Plus (SYBR Green) (TIANGEN). The qPCR reaction was performed on an ABI 7500 system (Applied Biosystems) with the following protocol: initial denaturation at 94°C for 3 min followed by 40 cycles of 95°C for 15 s, 60°C for 30 s, and 72°C for 30 s. The amplification efficiencies were determined by dissociation curve analysis using five twofold serial dilutions of *B. tabaci* cDNA template. In the follow-up study, only the primers with amplification efficiencies between 90 and 110% were used. The relative quantification was calculated according to the delta-delta Ct method (*63*) to

accurately analyze the expression of target genes. EF1-α, SDHA, and RPL29 were used as internal reference genes (*64*). Three independent biological replicates and four technical replicates were carried out for each type of sample.

dsRNA synthesis and RNAi assays

To determine the precise role of each OR gene in the localization of TYLCV-infected tomato plants, the expression of OR genes was inhibited through oral administration of double-stranded RNA (dsRNA) to adult *B. tabaci* MED. To prevent any potential missense effects, the SnapDragon tool (https://www.flyrnai.org/cgi-bin/RNAi_find_primers.pl) was used to design dsRNA primers (table S5), which were then synthesized in vitro through the T7 Ribomax Express RNAi system (Promega). RNAi was administered to adult *B. tabaci* through a feeding solution containing dsRNA (*62*). The solution was placed between two Parafilm layers, with each glass tube (50-mm long and 15 mm in diameter) containing 50 adults. Each feeding solution consisted of dsRNA (200 μl and 0.5 μg/μl). The effectiveness of RNAi was measured through qPCR, with adult *B. tabaci* being fed for 24 to 72 hours. The adult insects were either fed with dsRNA or the feeding solution without dsRNA for the specified duration (*65*).

Protein preparation and Western blot analysis

Samples were collected and homogenized using TRIzol reagent (Life Technologies). Protein extraction for Western blot analysis was done following the manufacturer's instructions. The antibody against the OR6 protein used for Western blots was generated from synthetic peptides (ABclonal, Wuhan, China) derived from respective specific amino acid sequences 150LSTVVSPLVRFVFETHDSFIVMPIWYPWDMLASPVRFWLAYVYESIVLWYTGVHYLHSGTLYFYAIATAKTRFHVLSDHIVNVAVQSDCSNPNEWKCSLKTEGKCKTYDINLMKDSER267. Two New Zealand White rabbits were immunized with each antigen. Rabbit serum potency was monitored, and all sera were collected after enzyme-linked immunosorbent assay (ELISA) validation. The best rabbit serum antigen was selected, purified on an affinity chromatography column, and validated using ELISA. The antibodies obtained were used for subsequent protein experiments. Protein samples (100 μg) were separated through gel electrophoresis and were transferred to polyvinylidene difluoride membranes (Millipore). Nonspecific binding sites on the membranes were blocked using 5% bovine serum albumin. Primary antibodies, rabbit anti-OR6 antibody (1:500) and rabbit anti–β-actin antibody (1:5000), were incubated separately with the blots in Tris Buffered Saline with Tween-20 (TBS-T) overnight at 4°C. Subsequently, the membranes were washed and then incubated with the anti-rabbit immunoglobulin G secondary antibody (1:5000) (EASYBIO Technology) for 1 hour at room temperature. Another wash was followed by immunological blot detection using an ECL kit (Thermo Fisher Scientific, 34096) (*66*, *67*). Western blot signals were quantified with the use of densitometry.

Protein structure prediction, MD simulation, and molecular docking

Protein structure prediction any analysis was carried out using the ROBETTA online platform, which offers a comprehensive suite of tools for both ab initio and comparative modeling of protein domains (*68*). MD simulations were performed using the Gromacs 2022.1 program at constant temperature and pressure as well as periodic boundary conditions (*69*, *70*). During MD simulations, hydrogen atoms were constrained using the LINear Constraint Solver (LINCS) algorithm, and electrostatic interactions were calculated using the Particle-mesh Ewald method (*71*, *72*). The V-rescale mutation coupling and Parrinello-Rahman method were used to control the simulated mutation to 298.15 K and the pressure to 1 bar (*73*, *74*). Then, the canonical ensemble and constant-pressure, constant-temperature equilibrium simulations were then carried out for 1 ns. Last, MD simulations were carried out for 100 ns for each of the systems, the conformations were saved every 10 ps, and the visualization of the simulation results was done by using the Gromacs embedded program and Visual Molecular Dynamics.

Molecular docking was implemented using the AutoDock 4.2.6 software package. With the coordinates of the docking box center set to the center of the protein wrapping the entire protein structure in its entirety, the number of lattice points in each of the *XYZ* directions sets to 100 × 100 × 100, the number of docking times sets to 50, and the rest of the parameters used as default values (*75*). The optimized, stable structure was then selected as the model for subsequent analysis.

Field trapping experiment

Three different tomato greenhouses, which had varying levels of spontaneous MED whitefly infestations, were selected for the field experiment, with differences in geographic location (Fig. 5A) and tomato varieties and developmental stages. Details were as follows:

1. Tomato greenhouse at the Vegetable Institute: The greenhouse is situated in the Vegetable and Flower Research Institute of the Chinese Academy of Agricultural Sciences, located in the Haidian District of Beijing, with an area of 300 m^2. The latitude and longitude of the greenhouse are 116.338855 and 39.969596, respectively. Shed A1 was planted with the Chinese Hybrid 9 tomato variety and was planted with the fifth crop. Shed A2 was planted with a different variety of tomato after the first crop had been harvested.

2. Tomato Shed at the Shunyi Suihang Base: It is located at the Shunyi District Agricultural Base in Beijing. The total area of the greenhouse is 500 m^2, and the specific geographic location is 116.760915 east longitude, 40.127585 north latitude. Shed B1 greenhouse housed the pink queen tomato, which had entered the fifth harvest cycle. Shed B2 greenhouse contained cherry tomato varieties, which were shortly after harvest replaced with seedlings. Shed B3 greenhouse contained the pink queen variety which had entered the fourth planting cycle.

3. Tomato greenhouse at Pinggu Guxing Base: The greenhouse is located in the Agricultural Base of Pinggu District, Beijing. The area of the greenhouse is 1000 m^2, and the latitude and longitude are 117.209017 and 40.141164. The tomato variety grown here was Rising Star 5. Shed C1 contained the third crop, and sheds C2 and C3 had the fifth crop.

In each shed, we placed 20 sticky boards (Fig. 5B), 10 of which were spiked with β-myrcene dissolved in CH_2Cl_2 (200 μl on a piece of filter paper, 2000 ng/μl) and 10 only received the solvent. The sticky boards were positioned in the middle of the two rows of tomato plants. One day after placing these traps, they were collected, and the number of whiteflies per boards was counted.

Statistical analyses

Statistical analyses were performed using SPSS software (Chicago, IL). The Wilk-Shapiro test was used to assess the normality of each

dataset. For data that followed a normal distribution, a two-tailed paired *t* test was used for analysis. Where data did not follow a parametric distribution, the Mann-Whitney test was used. Statistically significant differences between two groups are indicated with asterisks ($*P < 0.05$, $**P < 0.01$, and $***P < 0.001$).

Supplementary Materials

The PDF file includes:

Figs. S1 to S15
Tables S1 to S7
Legends for data S1 and S2

Other Supplementary Material for this manuscript includes the following:

Data S1 and S2

REFERENCES AND NOTES

1. V. R. Nicaise, Crop immunity against viruses: Outcomes and future challenges. *Front. Plant. Sci.* **5**, 660 (2014).
2. S. A. Hogenhout, E. D. Ammar, A. E. Whitfield, M. G. Redinbaugh, Insect vector interactions with persistently transmitted viruses. *Annu. Rev. Phytopathol.* **46**, 327–359 (2008).
3. M. S. Sisterson, Effects of insect-vector preference for healthy or infected plants on pathogen spread: Insights from a model. *J. Econ. Entonol.* **101**, 1–8 (2008).
4. Y. Wan, S. Hussain, A. Merchant, B. Xu, W. Xie, S. Wang, Y. Zhang, X. Zhou, Q. Wu, *Tomato spotted wilt orthotospovirus* influences the reproduction of its insect vector, western flower thrips, *Frankliniella occidentalis*, to facilitate transmission. *Pest Manag. Sci.* **76**, 2406–2414 (2020).
5. A. Fereres, M. F. Peñaflor, C. F. Favaro, K. E. Azevedo, C. H. Landi, N. K. Maluta, J. M. S. Bento, J. R. Lopes, Tomato infection by whitefly-transmitted circulative and non-circulative viruses induce contrasting changes in plant volatiles and vector behaviour. *Viruses* **8**, 225 (2016).
6. K. E. Mauck, C. M. De Moraes, M. C. Mescher, Deceptive chemical signals induced by a plant virus attract insect vectors to inferior hosts. *PNAS* **107**, 3600–3605 (2010).
7. R. Li, B. T. Weldegergis, J. Li, C. Jung, J. Qu, Y. Sun, H. Qian, C. Tee, M. van Loon, J. J. Dicke, N. H. Chua, S. S. Liu, J. Ye, Virulence factors of geminivirus interact with MYC2 to subvert plant resistance and promote vector performance. *Plant Cell* **26**, 4991–5008 (2014).
8. K. E. Mauck, Variation in virus effects on host plant phenotypes and insect vector behavior: What can it teach us about virus evolution? *Curr. Opin. Virol.* **21**, 114–123 (2016).
9. D. Shrestha, H. J. McAuslane, T. A. Ebert, F. A. Cervantes, S. T. Adkins, H. A. Smith, N. Dufault, S. E. Webb, Assessing the temporal effects of *squash vein yellowing virus* infection on settling and feeding behavior of *Bemisia tabaci* (MEAM1) (Hemiptera: Aleyrodidae). *J. Insect Sci.* **19**, 5 (2019).
10. S. F. Wang, H. Guo, F. Ge, Y. C. Sun, Apoptotic neurodegeneration in whitefly promotes the spread of TYLCV. *eLife* **9**, E56168 (2020).
11. H. He, J. Li, Z. Zhang, M. Yan, B. Zhang, C. Zhu, W. Yan, B. Shi, Y. Wang, C. Zhao, F. Yan, A plant virus enhances odorant-binding protein 5 (OBP5) in the vector whitefly for more actively olfactory orientation to the host plant. *Pest Manag.t Sci.* **79**, 1410–1419 (2023).
12. K. Hu, H. Yang, S. Liu, H. He, W. Ding, L. Qiu, Y. Li, Odorant-binding protein 2 is involved in the preference of *Sogatella furcifera* (Hemiptera: delphacidae) for rice plants infected with the *Southern Rice Black-Streaked Dwarf Virus*. *Fla. Entomol.* **102**, 353 (2019).
13. S. Li, C. Zhou, Y. Zhou, Olfactory co-receptor Orco stimulated by Rice stripe virus is essential for host seeking behavior in small brown planthopper. *Pest. Manag. Sci.* **75**, 187–194 (2019).
14. C. Carraher, J. Dalziel, M. D. Jordan, D. L. Christie, R. D. Newcomb, A. V. Kralicek, Towards an understanding of the structural basis for insect olfaction by odorant receptors. *Insect Biochem. Mol. Biol.* **66**, 31–41 (2015).
15. C. Y. Su, K. Menuz, J. R. Carlson, Olfactory perception: Receptors, cells, and circuits. *Cell* **139**, 45–59 (2009).
16. T. A. Franco, D. S. Oliveira, M. F. Moreira, W. S. Leal, A. C. Melo, Silencing the odorant receptor co-receptor *RproORco* affects the physiology and behavior of the Chagas disease vector *Rhodnius prolixus*. *Insect Biochem. Mol. Biol.* **69**, 82–90 (2016).
17. M. C. Larsson, A. I. Domingos, W. D. Jones, M. E. Chiappe, H. Amrein, L. B. Vosshall, Or83b encodes a broadly expressed odorant receptor essential for Drosophila olfaction. *Neuron* **43**, 703–714 (2004).
18. E. M. Neuhaus, G. Gisselmann, W. Zhang, R. Dooley, K. Störtkuhl, H. Hatt, Odorant receptor heterodimerization in the olfactory system of Drosophila melanogaster. *Nat. Neurosci.* **8**, 15–17 (2005).
19. J. A. Butterwick, J. Del Mármol, K. H. Kim, M. A. Kahlson, J. A. Rogow, T. Walz, V. Ruta, Cryo-EM structure of the insect olfactory receptor *ORco*. *Nature* **560**, 447–452 (2018).
20. E. A. Hallem, M. G. Ho, J. R. Carlson, The molecular basis of odor coding in the Drosophila antenna. *Cell* **117**, 965–979 (2004).
21. M. Guo, L. Du, Q. Chen, Y. Feng, J. Zhang, X. Zhang, K. Tian, S. Cao, T. Huang, E. Jacquin-Joly, G. Wang, Y. Liu, Odorant receptors for detecting flowering plant cues are functionally conserved across moths and butterflies. *Mol. Biol. Evol.* **38**, 1413–1427 (2021).
22. X. L. Liu, J. Zhang, Q. Yan, C. L. Miao, W. K. Han, W. Hou, K. Yang, B. S. Hansson, Y. C. Peng, J. M. Guo, H. Xu, C. Z. Wang, S. L. Dong, M. Knaden, The molecular basis of host selection in a crucifer-specialized moth. *Curr. Biol.* **30**, 4476–4482.e5 (2020).
23. Y. Wang, L. Qiu, B. Wang, Z. Guan, Z. Dong, J. Zhang, S. Cao, L. Yang, B. Wang, Z. Gong, L. Zhang, W. Ma, Z. Liu, D. Zhang, G. Wang, P. Yin, Structural basis for odorant recognition of the insect odorant receptor OR-Orco heterocomplex. *Science* **384**, 1453–1460 (2024).
24. J. D. Bohbot, J. C. Dickens, Characterization of an enantioselective odorant receptor in the yellow fever mosquito *Aedes aegypti*. *PLOS ONE* **4**, e7032 (2009).
25. Z. Zhao, J. L. Zung, A. Hinze, A. L. Kriete, A. Iqbal, M. A. Younger, B. J. Matthews, D. Merhof, S. Thiberge, R. Ignell, M. Strauch, C. S. McBride, Mosquito brains encode unique features of human odour to drive host seeking. *Nature* **605**, 706–712 (2022).
26. H. Liu, T. Liu, L. Xie, X. Wang, Y. Deng, C. H. Chen, A. A. James, X. G. Chen, Functional analysis of Orco and ORs in odor recognition in *Aedes albopictus*. *Parasit. Vectors* **9**, 363 (2016).
27. C. S. McBride, F. Baier, A. B. Omondi, S. A. Spitzer, J. Lutomiah, R. Sang, R. Ignell, L. B. Vosshall, Evolution of mosquito preference for humans linked to an odorant receptor. *Nature* **515**, 222–227 (2014).
28. M. R. V. Oliveira, T. J. Henneberry, P. Anderson, History, current status, and collaborative research projects for *Bemisia Tabaci*. *Crop Prot.* **20**, 709–723 (2001).
29. D. R. Jones, Plant viruses transmitted by whiteflies. *Eur. J. Plant Pathol.* **109**, 195–219 (2003).
30. P. J. De Barro, S. S. Liu, L. M. Boykin, A. B. Dinsdale, *Bemisia tabaci*: A statement of species status. *Annu. Rev. Entomol.* **56**, 1–19 (2011).
31. A. Prasad, N. Sharma, G. Hari-Gowthem, M. Muthamilarasan, M. Prasad, Tomato yellow leaf curl virus: Impact, challenges, and management. *Trends Plant Sci.* **25**, 897–911 (2020).
32. H. Zheng, W. Xie, S. Wang, Q. Wu, X. Zhou, Y. Zhang, Dynamic monitoring (B versus Q) and further resistance status of Q-type *Bemisia Tabaci* in China. *Crop Prot.* **94**, 115–122 (2017).
33. C. L. Guo, Y. Z. Zhu, Y. J. Zhang, M. A. Keller, T. X. Liu, D. Chu, Invasion biology and management of sweetpotato whitefly (Hemiptera: Aleyrodidae) in China. *J. Integr. Pest. Manag.* **12**, 2 (2021).
34. P. Lefeuvre, D. P. Martin, G. Harkins, P. Lemey, A. J. Gray, S. Meredith, F. Lakay, A. Monjane, J. M. Lett, A. Varsani, J. Heydarnejad, The spread of tomato yellow leaf curl virus from the Middle East to the World. *PLOS Pathog.* **6**, E1001164 (2010).
35. Y. Fang, X. Jiao, W. Xie, S. Wang, Q. Wu, X. Shi, G. Chen, Q. Su, X. Yang, H. Pan, Y. Zhang, Tomato yellow leaf curl virus alters the host preferences of its vector *Bemisia Tabaci*. *Sci. Rep.* **3**, 2876 (2013).
36. B. K. Roosien, R. Gomulkiewicz, L. L. Ingwell, N. A. Bosque-Pérez, D. Rajabaskar, S. D. Eigenbrode, Conditional vector preference aids the spread of plant pathogens: Results from a model. *Environ. Entomol.* **42**, 1299–1308 (2013).
37. M. J. Jeger, The epidemiology of plant virus disease: Towards a new synthesis. *Plants (Basel)* **9**, 1768 (2020).
38. V. Falara, T. A. Akhtar, T. T. Nguyen, E. A. Spyropoulou, P. M. Bleeker, I. Schauvinhold, Y. Matsuba, M. E. Bonini, A. L. Schilmiller, R. L. Last, R. C. Schuurink, E. Pichersky, The tomato terpene synthase gene family. *Plant Physiol.* **157**, 770–789 (2011).
39. A. E. Whitfield, B. W. Falk, D. Rotenberg, Insect vector-mediated transmission of plant viruses. *Virology* **480**, 278–289 (2015).
40. K. E. Mauck, J. Kenney, Q. Chesnais, Progress and challenges in identifying molecular mechanisms underlying host and vector manipulation by plant viruses. *Curr. Opin. Insect Sci.* **33**, 7–18 (2019).
41. C. L. Casteel, C. Yang, A. C. Nanduri, H. N. De Jong, S. A. Whitham, G. Jander, The NIa-Pro protein of Turnip mosaic virus improves growth and reproduction of the aphid vector, *Myzus persicae* (green peach aphid). *Plant J.* **77**, 653–663 (2014).
42. J. B. Luan, X. W. Wang, J. Colvin, S. S. Liu, Plant-mediated whitefly-begomovirus interactions: Research progress and future prospects. *Bull. Entomol. Res.* **104**, 267–276 (2014).
43. X. Liu, G. Chen, Y. Zhang, W. Xie, Q. Wu, S. Wang, Virus-infected plants altered the host selection of *Encarsia formosa*, a parasitoid of whiteflies. *Front. Physiol.* **8**, 937 (2017).
44. G. J. Hong, X. Y. Xue, Y. B. Mao, L. J. Wang, X. Y. Chen, Arabidopsis MYC2 interacts with DELLA proteins in regulating sesquiterpene synthase gene expression. *Plant Cell* **24**, 2635–2648 (2012).
45. E. A. Spyropoulou, M. A. Haring, R. C. Schuurink, RNA sequencing on Solanum lycopersicum trichomes identifies transcription factors that activate terpene synthase promoters. *BMC Genomics* **15**, 402 (2014).
46. F. Schweizer, P. Fernández-Calvo, M. Zander, M. Diez-Diaz, S. Fonseca, G. Glauser, M. G. Lewsey, J. R. Ecker, R. Solano, P. Reymond, Arabidopsis basic helix-loop-helix transcription factors MYC2, MYC3, and MYC4 regulate glucosinolate biosynthesis, insect performance, and feeding behavior. *Plant Cell* **25**, 3117–3132 (2013).

47. J. S. Thaler, P. T. Humphrey, N. K. Whiteman, Evolution of jasmonate and salicylate signal crosstalk. *Trends Plant Sci.* **17**, 260–270 (2012).
48. S. H. Spoel, J. S. Johnson, X. Dong, Regulation of tradeoffs between plant defenses against pathogens with different lifestyles. *Proc. Natl. Acad. Sci. U.S.A.* **104**, 18842–18847 (2007).
49. P. Engsontia, U. Sangket, W. Chotigeat, C. Satasook, Molecular evolution of the odorant and gustatory receptor genes in lepidopteran insects: Implications for their adaptation and speciation. *J. Mol. Evol.* **79**, 21–39 (2014).
50. S. I. Eyun, H. Y. Soh, M. Posavi, J. B. Munro, D. S. T. Hughes, S. C. Murali, J. Qu, S. Dugan, S. L. Lee, H. Chao, Evolutionary history of chemosensory-related gene families across the Arthropoda. *Mol. Biol. Evol.* **34**, 1838–1862 (2017).
51. H. M. Robertson, Molecular evolution of the major arthropod chemoreceptor gene families. *Annu. Rev. Entomol.* **64**, 227–242 (2019).
52. S. S. Liu, P. J. De Barro, J. Xu, J. B. Luan, L. S. Zang, Y. M. Ruan, F. H. Wan, Asymmetric mating interactions drive widespread invasion and displacement in a whitefly. *Science* **318**, 1769–1772 (2007).
53. B. M. Liu, F. M. Yan, D. Chu, H. P. Pan, X. G. Jiao, W. Xie, Q. J. Wu, S. L. Wang, B. Y. Xu, X. G. Zhou, Y. J. Zhang, Difference in feeding behaviors of two invasive whiteflies on host plants with different suitability: Implication for competitive displacement. *Int. J. Biol. Sci.* **8**, 697–706 (2012).
54. W. H. Jayasinghe, H. Kim, Y. Nakada, C. Masuta, A plant virus satellite RNA directly accelerates wing formation in its insect vector for spread. *Nat. Commun.* **12**, 7087 (2021).
55. S. Ray, C. L. Casteel, Effector-mediated plant-virus-vector interactions. *Plant Cell* **34**, 1514–1531 (2022).
56. D. Chu, F. Wan, Y. Zhang, J. Brown, Change in the biotype composition of *Bemisia Tabaci* in Shandong Province of China from 2005 to 2008. *Environ. Entomol.* **39**, 1028–1036 (2010).
57. H. Guo, L. Gu, F. Liu, F. Chen, F. Ge, Y. Sun, Aphid-borne viral spread is enhanced by virus-induced accumulation of plant reactive oxygen species. *Plant Physiol.* **179**, 143–155 (2019).
58. P. J. Zhang, J. N. Wei, C. Zhao, Y. F. Zhang, C. Y. Li, S. S. Liu, M. Dicke, X. P. Yu, T. C. J. Turlings, Airborne host-plant manipulation by whiteflies via an inducible blend of plant volatiles. *Proc. Natl. Acad. Sci. U.S.A.* **116**, 7387–7396 (2019).
59. I. W. Keesey, S. Koerte, M. A. Khallaf, T. Retzke, A. Guillou, E. Grosse-Wilde, N. Buchon, M. Knaden, B. S. Hansson, Pathogenic bacteria enhance dispersal through alteration of Drosophila social communication. *Nat. Commun.* **8**, 265 (2017).
60. R. Li, X. Wang, S. Zhang, X. Liu, Z. Zhou, Z. Liu, K. Wang, Y. Tian, H. Wang, Y. Zhang, X. Cui, Two zinc-finger proteins control the initiation and elongation of long stalk trichomes in tomato. *J. Genet. Genom.* **48**, 1057–1069 (2021).
61. W. Xie, Q. Wu, S. Wang, X. Jiao, L. Guo, X. Zhou, Y. Zhang, Transcriptome analysis of host-associated differentiation in *Bemisia Tabaci* (Hemiptera: Aleyrodidae). *Front. Physiol.* **5**, 487 (2014).
62. P. Liang, J. Ning, W. Wang, P. Zhu, L. Gui, W. Xie, Y. J. Zhang, Catalase promotes whitefly adaptation to high temperature by eliminating reactive oxygen species. *Insect Sci.* **30**, 1293–1308 (2023).
63. K. J. Livak, T. D. Schmittgen, Analysis of relative gene expression data using real-time quantitative PCR and the $2^{-\Delta\Delta C}_{T}$ method. *Methods* **25**, 402–408 (2001).
64. R. Li, S. Afsheen, Z. Xin, X. Han, Y. Lou, OsNPR1 negatively regulates herbivore-induced JA and ethylene signaling and plant resistance to a chewing herbivore in rice. *Physiol. Plant* **147**, 340–351 (2013).
65. J. X. Xia, Z. Guo, Z. Yang, H. Han, S. Wang, H. Xu, X. Yang, F. Yang, Q. Wu, W. Xie, X. Zhou, W. Dermauw, T. C. J. Turlings, Y. J. Zhang, Whitefly hijacks a plant detoxification gene that neutralizes plant toxins. *Cell* **184**, 1693–1705 (2021).
66. C. Gong, Z. Guo, Y. Hu, Z. Yang, J. Xia, X. Yang, W. Xie, S. Wang, Q. Wu, W. Ye, X. Zhou, T. C. J. Turlings, Y. J. Zhang, A horizontally transferred plant fatty acid desaturase gene steers whitefly reproduction. *Adv. Sci.* **11**, e2306653 (2024).
67. Z. Z. Yang, Z. Guo, C. Gong, J. Xia, Y. Hu, J. Zhong, X. Yang, W. Xie, S. Wang, Q. Wu, W. Ye, B. Liu, X. Zhou, T. C. J. Turlings, Y. J. Zhang, Two horizontally acquired bacterial genes steer the exceptionally efficient and flexible nitrogenous waste cycling in whiteflies. *Sci. Adv.* **10**, eadi3105 (2024).
68. J. Yang, I. Anishchenko, H. Park, Z. Peng, S. Ovchinnikov, D. Baker, Improved protein structure prediction using predicted interresidue orientations. *Proc. Natl. Acad. Sci. U.S.A.* **117**, 1496–1503 (2020).
69. D. Van Der Spoel, E. Lindahl, B. Hess, G. Groenhof, A. E. Mark, H. J. Berendsen, GROMACS: Fast, flexible, and free. *J. Comput. Chem.* **26**, 1701–1718 (2005).
70. W. L. Jorgensen, J. Chandrasekhar, J. D. Madura, Comparison of simple potential functions for simulating liquid water. *J. Chem. Phys.* **79**, 926–935 (1983).
71. B. Hess, H. Bekker, H. J. C. Berendsen, J. G. E. M. Fraaije, LINCS: A linear constraint solver for molecular simulations. *J. Chem. Theor. Comput.* **18**, 1463–1472 (1997).
72. T. A. Darden, D. M. York, L. G. Pedersen, Particle mesh Ewald-an N.log(N) method for Ewald sums in large systems. *J. Chem. Phys.* **98**, 10089–10092 (1993).
73. H. J. C. Berendsen, J. P. M. Postma, W. F. Van Gunsteren, A. Di Nola, J. R. Haak, Molecular dynamics with coupling to an external bath. *J. Chem. Phys.* **81**, 3684–3690 (1984).
74. R. Martonák, A. Laio, M. Parrinello, Predicting crystal structures: The Parrinello-Rahman method revisited. *Phys. Rev. Lett.* **90**, 075503 (2003).
75. J. A. Maier, C. Martinez, K. Kasavajhala, L. Wickstrom, K. E. Hauser, C. Simmerling, ff14SB: Improving the accuracy of protein side chain and backbone parameters from ff99SB. *J. Chem. Theor. Comput.* **11**, 3696–3713 (2015).

Acknowledgments: We thank X. Zhou for providing the original strain of TYLCV. This work was partially supported by the C. W. Kearns, C. L. Metcalf, and W. P. Flint Endowed Chair Professorship in Insect Toxicology to X.Z. **Funding:** This work was supported by National Key R&D Program of China (2022YFD1400800), National Natural Science Foundation of China (32272534, 32221004, and 32202282), Hainan Major Science and Technology Project (ZDKJ2021007), Innovational Fund for Scientific and Technological Personnel of Hainan Province (KJRC2023C45), and Science and Technology special fund of Hainan Province (ZDYF2024XDNY250), Central Public-interest Scientific Institution Basal Research Fund (Y2023XK15 and Y2024XK01), Hubei Key Laboratory of Edible Wild Plants Conservation and Utilization (EWPL202309), The Earmarked Fund for CARS (CARS-23), and The Science and Technology Innovation Program of the Chinese Academy of Agricultural Sciences (CAAS-ASTIP-IVFCAAS). The contribution by T.C.J.T. was supported by a European Research Council Advanced Grant (788949). **Author contributions:** Conceptualization: P.L., Y.Ze., Q.W., Q.S., X.Z., T.C.J.T., W.X., and Y.Zh. Methodology: P.L., Y.Ze., J.N., X.W., W.W., J.R., Q.W., S.W., Z.G., X.Z., W.X., and Y.Zh. Investigation: P.L., Y.Ze., J.N., X.W., W.W., and W.X. Data curation: Y.Ze. Validation: P.L., Y.Ze., X.W., W.W., X.Y., T.C.J.T., W.X., and Y.Zh. Formal analysis: P.L., Y.Ze., J.N., and Y.Zh. Resources: Y.Ze., W.W., Q.W., S.W., W.X., and Y.Zh. Visualization: P.L., Y.Ze., Q.W., S.W., Q.S., T.C.J.T., and W.X. Supervision: Q.W., T.C.J.T., W.X., and Y.Zh. Funding acquisition: J.R., Q.W., S.W., Z.G., W.X., and Y.Zh. Project administration: Q.W., W.X., and Y.Zh. Writing—original draft: P.L., Y.Ze., Q.W., Q.S., T.C.J.T., W.X., and Y.Zh. Writing—review and editing: P.L., Y.Ze., Q.W., S.W., Z.G., Q.S., X.Z., T.C.J.T., W.X., and Y.Zh. **Competing interests:** The authors declare that they have no competing interests. **Data and materials availability:** All data needed to evaluate the conclusions in the paper are present in the paper and/or the Supplementary Materials.

Submitted 1 July 2024
Accepted 27 January 2025
Published 28 February 2025
10.1126/sciadv.adr4563